Crystal structure of tezacaftor Form A, $C_{26}H_{27}F_3N_2O_6$

James A. Kaduk,[1,2,a] Amy M. Gindhart,[3] and Thomas N. Blanton[3]
[1]*North Central College, 131 S. Loomis St., Naperville, Illinois 60540, USA*
[2]*Illinois Institute of Technology, 3101 S. Dearborn St., Chicago, Illinois 60616, USA*
[3]*ICDD, 12 Campus Blvd., Newtown Square, Pennsylvania 19073-3273, USA*

(Received 6 November 2020; accepted 27 December 2020)

The crystal structure of tezacaftor Form A has been solved and refined using synchrotron X-ray powder diffraction data, and optimized using density functional techniques. Tezacaftor Form A crystallizes in space group *C*2 (#5) with $a = 21.05142(6)$, $b = 6.60851(2)$, $c = 17.76032(5)$ Å, $\beta = 95.8255(2)°$, $V = 2458.027(7)$ Å^3, and $Z = 4$. The crystal structure is dominated by van der Waals interactions. O–H···O hydrogen bonds link the molecules in chains along the *b*-axis, and there are a variety of C–H···O hydrogen bonds, both intra- and intermolecular. The powder pattern has been submitted to ICDD® for inclusion in the Powder Diffraction File™ (PDF®). © *2021 International Centre for Diffraction Data*. [doi:10.1017/S0885715621000051]

Key words: tezacaftor, Symdeko, Rietveld refinement, density functional theory

I. INTRODUCTION

Tezacaftor, in combination with ivacaftor, is sold as Symdeko, and used to treat cystic fibrosis. Its function is to correct the positioning of the cystic fibrosis transmembrane regulator (CFTR) protein on a mutated cell surface to permit proper channel formation and improved flow of water and salts across the cell membrane. The IUPAC name (CAS Registry number 1152311-62-0) is 1-(2,2-difluoro-1,3-benzodioxol-5-yl)-*N*-[1-[(2R)-2,3-dihydroxypropyl]-6-fluoro-2-(1-hydroxy-2-methylpropan-2-yl)indol-5-yl]cyclopropane-1-carboxamide. The molecular structure of tezacaftor is illustrated in Figure 1.

The synthetic routes and crystalline forms of tezacaftor have been reviewed by Hughes (2019). X-ray powder diffraction data have been reported in EP2563778B1 (Keshavarz-Shokri *et al.*, 2016) and many equivalent patents. A single-crystal study was carried out, but no atom coordinates are reported in the patent. A powder pattern for amorphous tezacaftor is also reported.

This work was carried out as part of a project (Kaduk *et al.*, 2014) to determine the crystal structures of large-volume commercial pharmaceuticals and include high-quality powder diffraction data for these pharmaceuticals in the Powder Diffraction File (Gates-Rector and Blanton, 2019).

II. EXPERIMENTAL

The sample was a commercial reagent, purchased from Sigma (Lot #10611), and was used as-received. The white powder was packed into a 1.5-mm diameter Kapton capillary and rotated during the measurement at ~50 Hz. The powder pattern was measured at 295 K at beam line 11-BM (Lee *et al.*, 2008; Wang *et al.*, 2008) of the Advanced Photon Source at Argonne National Laboratory using a wavelength of 0.457899 Å from 0.5° to 50° 2θ with a step size of 0.001° and a counting time of 0.1 s step^{-1}.

The pattern was indexed on a *C*-centered monoclinic unit cell with $a = 21.05637$, $b = 6.61006$, $c = 17.75860$ Å, $\beta = 95.82°$, $V = 2458.92$ Å^3, and $Z = 4$ using Jade Pro 7.8 (MDI, 2020). The cell volume indicated $Z = 4$, and since tezacaftor is a chiral molecule, the space group was assumed to be *C*2, which was confirmed by successful solution and refinement of the structure. A reduced cell search in the Cambridge Structural Database (Groom *et al.*, 2016) yielded three hits, but no structures for tezacaftor derivatives.

A tezacaftor molecule was downloaded from PubChem as Conformer3D_CID_46199646.sdf. It was converted to a .mol2 file using Materials Studio (Dassault, 2020) and converted into a Fenske-Hall *Z*-matrix using OpenBabel (O'Boyle *et al.*, 2011). The structure was solved by Monte Carlo simulated annealing techniques as implemented in DASH (David *et al.*, 2006). A 010 preferred orientation coefficient was also included, but no Mogul Distribution Bias was applied. The success rate was ~40% of the 100 runs.

Rietveld refinement was carried out using GSAS-II (Toby and Von Dreele, 2013). Only the 1.0–25.0° portion of the pattern was included in the refinement ($d_{min} = 1.057$ Å), with an excluded region 1.60–2.0° to ignore a peak from the Kapton capillary. All non-H bond distances and angles were subjected to restraints, based on a Mercury/Mogul Geometry Check (Bruno *et al.*, 2004; Sykes *et al.*, 2011) of the model. The Mogul average and standard deviation for each quantity were used as the restraint parameters. The restraints contributed 8.5% to the final χ^2. The *y*-coordinate of F1 was fixed to define the origin. The hydrogen atoms were included in calculated positions, which were recalculated during the refinement using Materials Studio (Dassault, 2020). The U_{iso} were grouped by chemical similarity. The U_{iso} of the hydrogen atoms were constrained to be 1.3× that of the heavy atoms to which there are attached. The background was modeled

[a]Author to whom correspondence should be addressed. Electronic mail: kaduk@polycrystallography.com

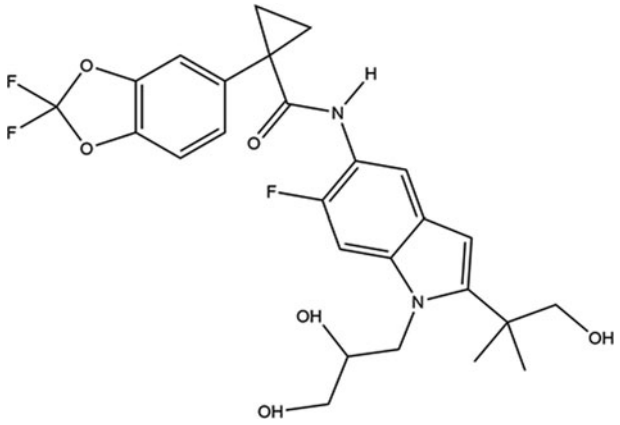

Figure 1. The molecular structure of tezacaftor.

using a 6-term shifted Chebyshev polynomial, along with a peak at 1.71° and 5.45° to model the scattering from the Kapton capillary and any amorphous component of the sample. The peak profiles were described using the generalized microstrain model, and a second-order spherical harmonic preferred orientation model was included. A few additional peaks indicated the presence of a second crystalline phase, which was identified as NaCl. Its concentration refined to 0.44(1) wt%.

The final refinement of 144 variables using 23 337 observations and 106 restraints yielded the residuals $R_{wp} = 0.0696$ and GOF = 1.45. The largest peak (1.43 Å from F3) and hole (2.04 Å from C12) in the difference Fourier map were 0.26 and −0.21(5) eÅ^{-3}, respectively. The largest errors in the fit (Figure 2) are in the positions and shapes of some of the low-angle peaks, and may indicate subtle changes in the beam during the measurement.

A density functional geometry optimization (fixed experimental unit cell) was carried using CRYSTAL14 (Dovesi *et al.*, 2014). The basis sets for the H, C, N, and O atoms were those of Gatti *et al.* (1994), and that for F was that of Peintinger *et al.* (2013). The calculation was run on eight 2.1 GHz Xeon cores (each with 6 GB RAM) of a 304-core Dell Linux cluster at IIT, using 8 *k*-points and the B3LYP functional, and took ∼73 h.

III. RESULTS AND DISCUSSION

Hughes notes that only one crystalline form (Form A) of tezacaftor has been reported. The synchrotron pattern from this current study (Figure 3) matches well with both the observed and calculated patterns reported by Keshavarz-Shokri *et al.* (2016; Vertex), confirming that we have studied the same material. The lattice parameters of the two determinations (Table I) differ slightly. Those from this synchrotron powder study are more precise than those from the single-crystal study. The current lattice parameters are slightly smaller, probably reflecting differences in preparations.

The refined atom coordinates of tezacaftor Form A and the coordinates from the density functional theory (DFT) optimization are reported in the CIFs deposited with ICDD. The root-mean-square (rms) Cartesian displacement of the non-hydrogen atoms in the Rietveld-refined and DFT-optimized structures is 0.201 Å (Figure 4), within the normal range for correct structures (van de Streek and Neumann, 2014). The maximum difference is 0.508 Å, at O7, and reflects a difference in the conformation of that branch of the molecule. This discussion concentrates on the DFT-optimized structure, as we believe it is more reliable. The asymmetric unit (with atom numbering) is illustrated in Figure 5, and the crystal structure is presented in Figure 6.

The crystal structure (Figure 6) is apparently dominated by van der Waals interactions. The O–H···O hydrogen bonds link the molecules in *C*1,1(10) chains (Etter, 1990; Bernstein *et al.*, 1995; Shields *et al.*, 2000) along the *b*-axis. Visually, there are π···π stacking interactions roughly parallel

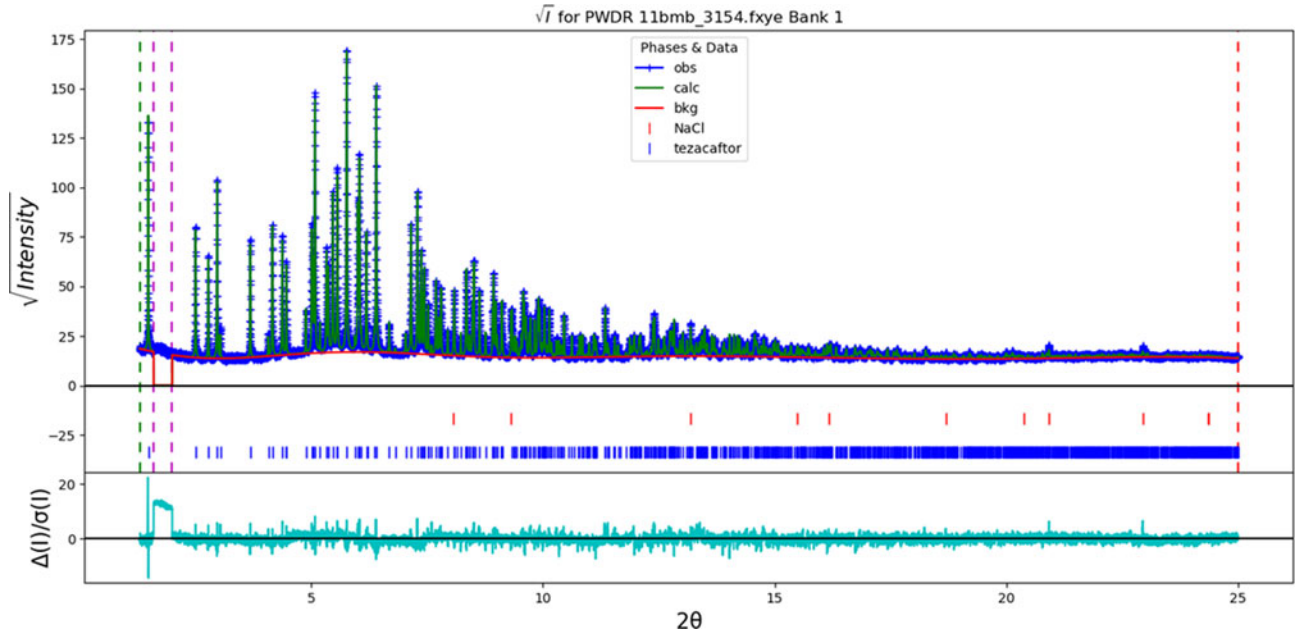

Figure 2. The Rietveld plot for the refinement of tezacaftor Form A. The blue crosses represent the observed data points, and the green line is the calculated pattern. The cyan curve is the normalized error plot. The vertical scale is the square root of the intensity.

https://doi.org/10.1017/S0885715621000051 Published online by Cambridge University Press

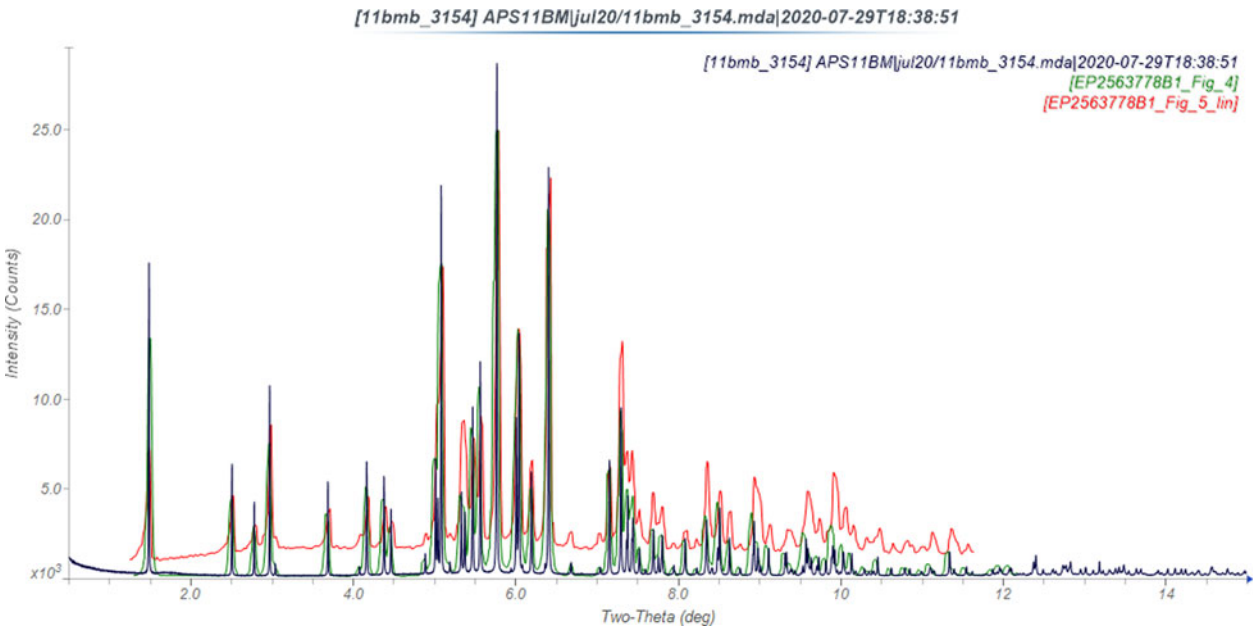

Figure 3. Comparison of the synchrotron pattern of tezacaftor Form A to the patterns reported by Keshavarz-Shokri *et al.* (2016). The experimental pattern from Figure 5 of the patent is presented in red, and the pattern of Figure 4 of the patent (calculated from the single-crystal structure) is given in green. The published patterns were digitized using UN-SCAN-IT (Silk Scientific, 2013) and scaled to the synchrotron wavelength of 0.457899 Å using MDI JADE Pro (MDI, 2020).

TABLE I. Lattice parameters (space group *C*2) of tezacaftor.

Source	This work	Keshavarz-Shokri *et al.* (2016)	Ratio
T (K)	295	295	
a (Å)	21.05142(6)	21.0952(16)	0.99793
b (Å)	6.60851(2)	6.6287(5)	0.99695
c (Å)	17.76032(5)	17.7917(15)	0.99824
β (°)	95.8255(2)	95.867(3)	
V (Å^3)	2458.027(7)	2474.8(3)	0.99322

to the 1-11 plane, but the analysis of the Mulliken overlap populations does not pinpoint them.

Almost all of the bond distances, angles, and torsion angles fall within the normal ranges indicated by a Mercury/Mogul Geometry check (Macrae *et al.*, 2020). The F3–C36 bond distance of 1.385 Å (average = 1.325(16) Å, *Z*-score = 3.6) is flagged as unusual. The equivalent F2–C36 bond has a *Z*-score of only 1.9. The C25–N11–C22 angle of 108.2° is slightly unusual (average = 111.2(9)°, *Z*-score = 3.1), but the uncertainty on the average is exceptionally low, making the *Z*-score artificially high. The C27–C20–N10–C16 and C30–C20–N10–C16 torsion angles are flagged as unusual. These both occur in tails of distributions and represent rotation around the C20–N10 amide bond. They represent the orientation of two parts of the molecule, which seems to be unusual. The C16–C12–C15–C17 and C16–C12–C15–C18 torsions are also noted as unusual, but these are part of a broad distribution with relatively few hits.

Quantum chemical geometry optimization of the isolate tezacaftor molecule (DFT/B3LYP/6-31G*/water) using Spartan '18 (Wavefunction, 2020) indicated that the observed solid-state conformation is 7.0 kcal mol^{-1} higher in energy than the local minimum (Figure 7), and that the conformations

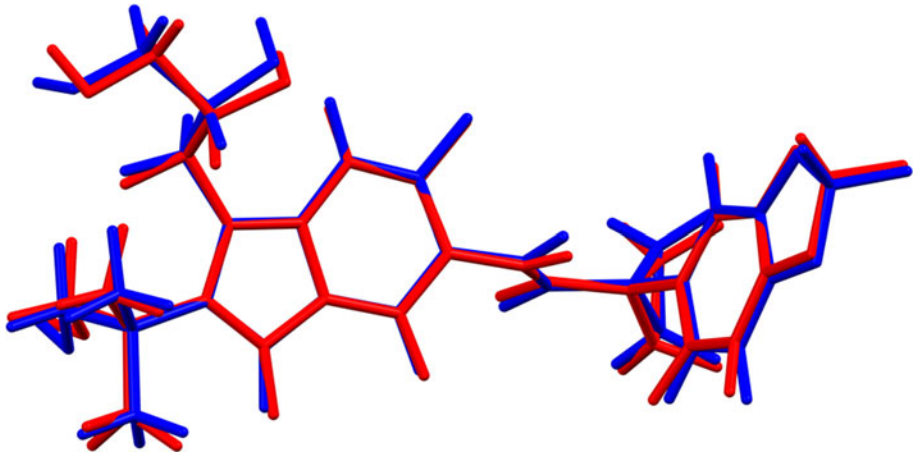

Figure 4. Comparison of the Rietveld-refined (red) and VASP-optimized (blue) structures of tezacaftor Form A. The rms Cartesian displacement is 0.201 Å.

https://doi.org/10.1017/S0885715621000051 Published online by Cambridge University Press

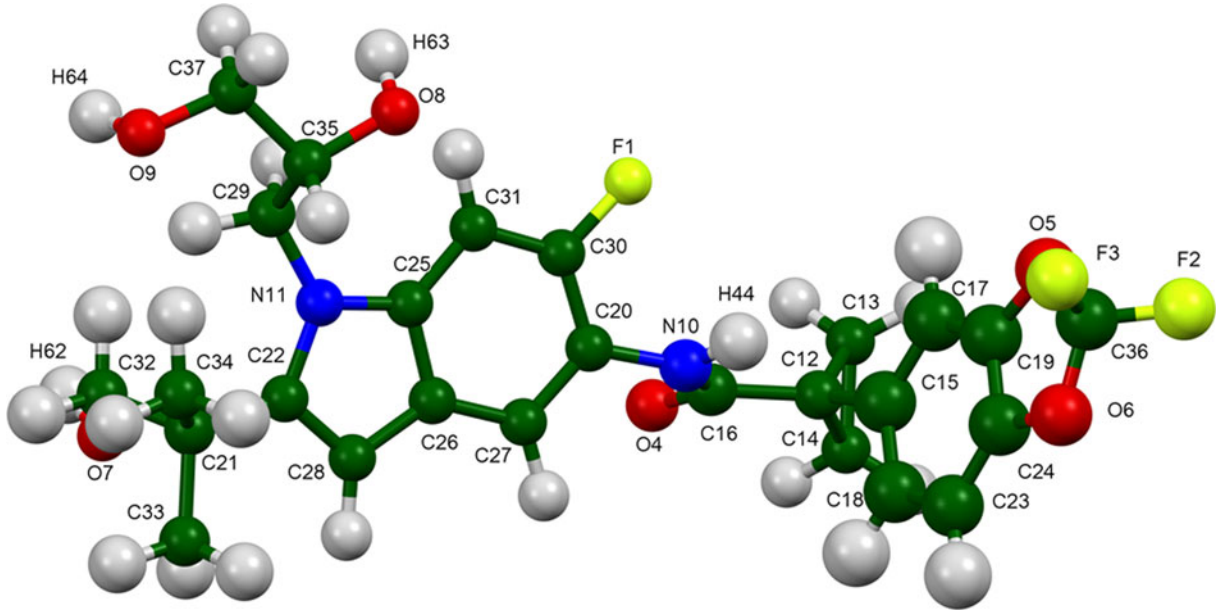

Figure 5. The asymmetric unit of tezacaftor Form A, with the atom numbering. The atoms are represented by 50% probability spheroids.

differ significantly. The rms Cartesian displacement is 1.793 Å. In particular, the C30–C20–N10–C16 torsion angle is −177.0° in the local minimum structure, consistent with the expectations from the Mogul geometry analysis. The local minimum conformation also differs from the global minimum energy conformation from a molecular mechanics (force field) analysis (Figure 8). Apparently both inter- and intramolecular interactions contribute significantly to determining the observed solid-state conformation.

Analysis of the contributions to the total crystal energy using the Forcite module of Materials Studio (Dassault, 2020) suggests that angle deformation terms are the dominant contributions to the intramolecular deformation energy, as expected for a molecule, which contains fused ring systems and a cyclopropane ring. The intermolecular energy is dominated by electrostatic attractions, which in this force-field-based analysis include hydrogen bonds. The hydrogen bonds are better analyzed using the results of the DFT calculation.

Although there are hydrogen bonds in the structure (Table II), they do not seem especially important to the crystal energy. Surprisingly, only the hydroxyl group O7–H62 acts as a hydrogen bond donor, while the other hydroxyl groups O8

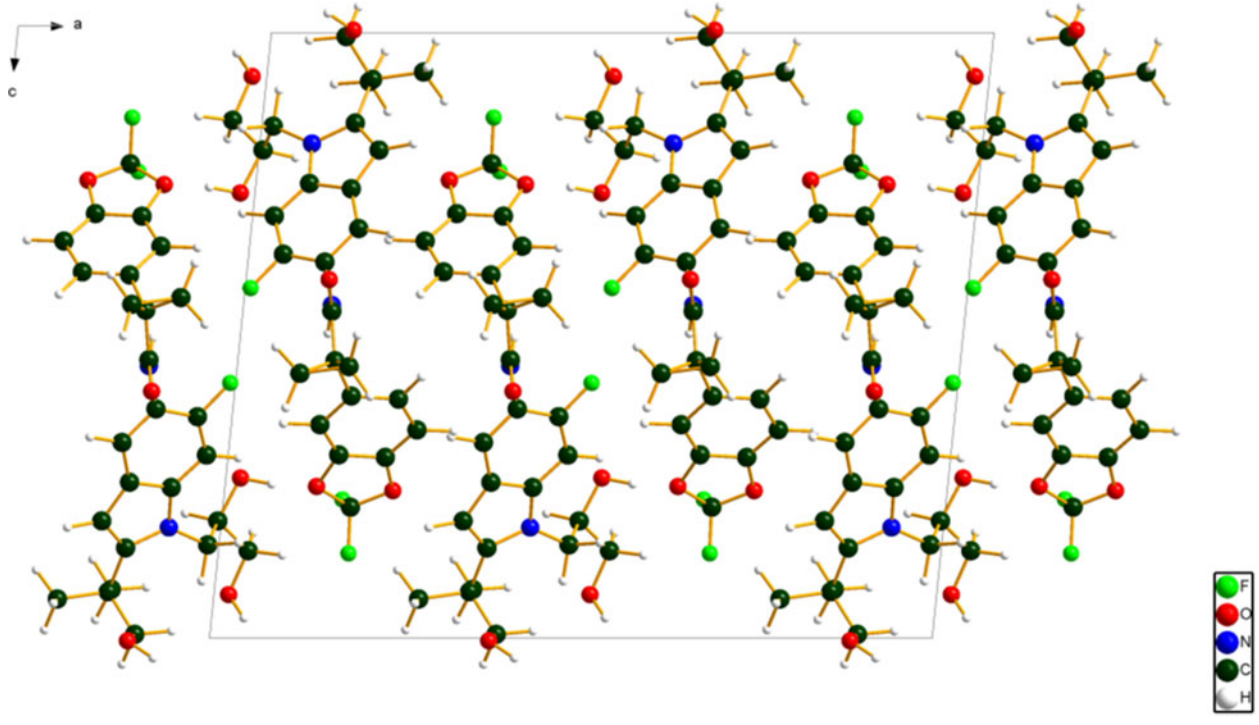

Figure 6. The crystal structure of tezacaftor Form A, viewed down the *b*-axis.

https://doi.org/10.1017/S0885715621000051 Published online by Cambridge University Press

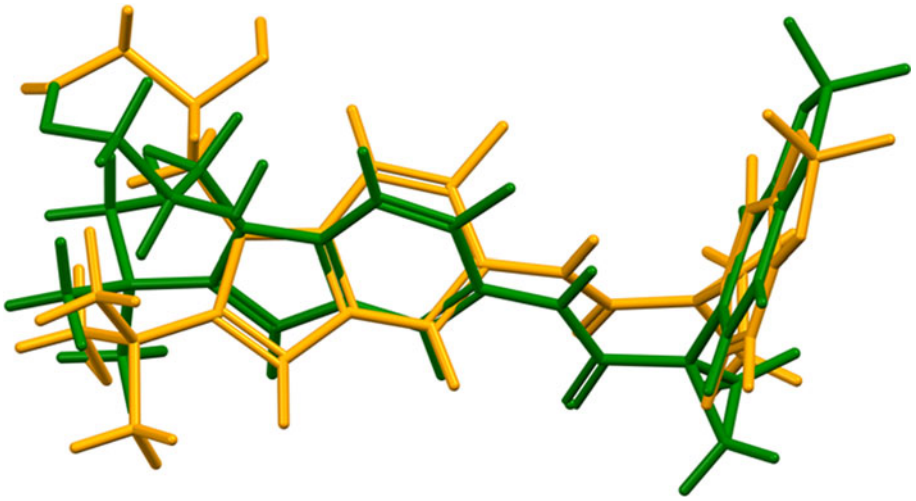

Figure 7. Comparison of the local minimum-energy (green) conformation and the DFT-optimized conformation (orange) in tezacaftor Form A.

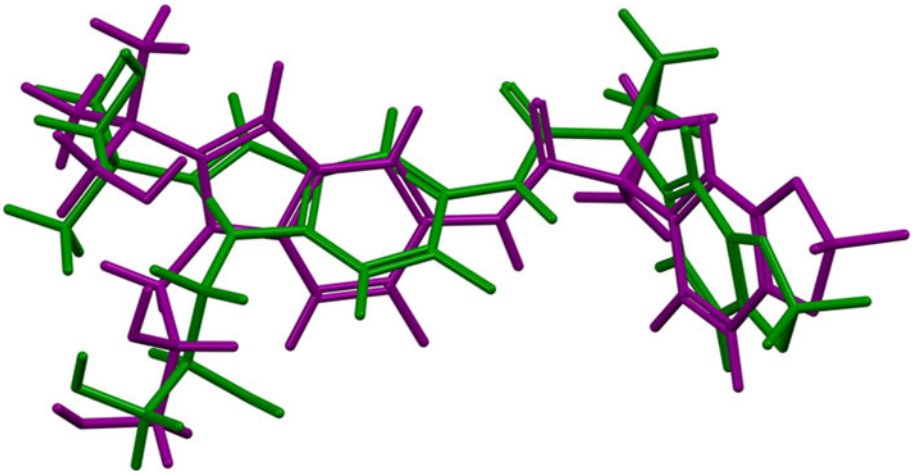

Figure 8. Comparison of the local minimum-energy conformation (green) and the global minimum-energy conformation (purple) of tezacaftor.

TABLE II. Hydrogen bonds (CRYSTAL14) in tezacaftor.

H-bond	D-H (Å)	H···A (Å)	D···A (Å)	D-H···A (°)	Overlap (*e*)	*E* (kcal mol^{-1})
O7–H62···O9	0.971	1.937	2.846	154.8	0.050	12.2
C33–H55···O7	1.091	2.455[a]	2.820	97.9	0.010	
C34–H53···O9	1.093	2.597[a]	3.681	171.4	0.013	
C31–H50···O8	1.076	2.326[a]	3.040	122.3	0.021	
C29–H49···O9	1.086	2.519[a]	3.007	106.1	0.016	
C17–H42···O8	1.082	2.475	3.217	124.7	0.017	
C23–H45···O4	1.084	2.155	3.106	145.0	0.027	
C14–H38···O4	1.084	2.437[a]	2.825	99.5	0.017	
N10–H44···C15	1.011	2.388[a]	2.832	105.6	0.011	

[a]Intramolecular.

and O9 act as acceptors in multiple C–H···O hydrogen bonds, many of which are intramolecular. The energy of the O–H···O hydrogen bond was calculated using the correlation of Rammohan and Kaduk (2018). The carbonyl group O4 acts as an acceptor in two C–H···O hydrogen bonds, one of which is intramolecular. There is an intramolecular N–H···C hydrogen bond between the amide nitrogen N10 and C15 in the cyclopropane ring. Examining both the Mulliken overlap populations and the short intermolecular contact suggest the possibility of a variety of weaker interactions.

The volume enclosed by the Hirshfeld surface (Figure 9; Hirshfeld, 1977; Turner *et al.*, 2017) is 605.65 Å^3, 98.55% of 1/4 the unit cell volume. The molecules are, thus, not tightly packed. All of the significant close contacts (red in Figure 9) involve the hydrogen bonds. The volume/non-hydrogen atom is 16.6 Å^3.

https://doi.org/10.1017/S0885715621000051 Published online by Cambridge University Press

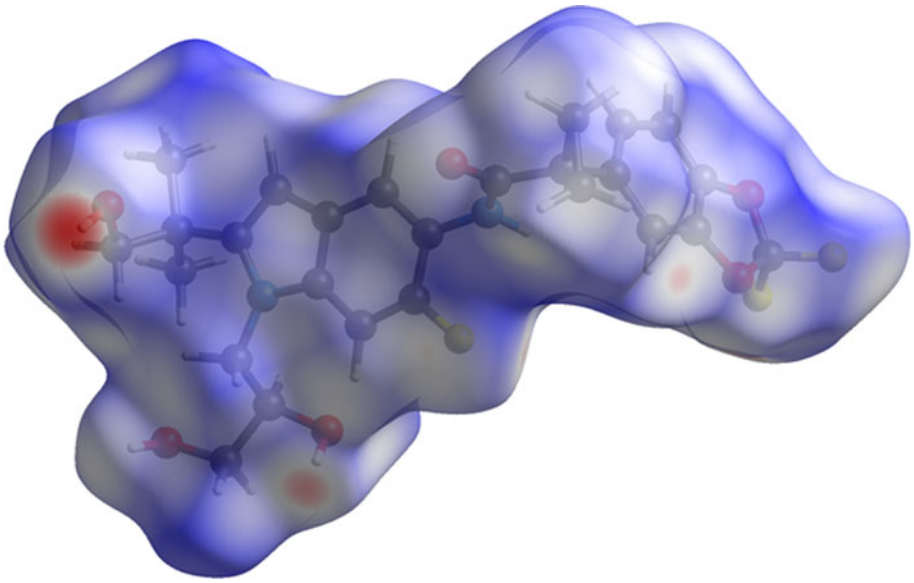

Figure 9. The Hirshfeld surface of tezacaftor Form A. Intermolecular contacts longer than the sums of the van der Waals radii are colored blue, and contacts shorter than the sums of the radii are colored red. Contacts equal to the sums of radii are white.

The Bravais–Friedel–Donnay–Harker (Bravais, 1866; Friedel, 1907; Donnay and Harker, 1937) morphology suggests that we might expect platy morphology for tezacaftor Form A, with {001} as the principal faces. A second-order spherical harmonic model for preferred orientation was incorporated into the refinement. The texture index was only 1.001(0), indicating that preferred orientation was slight in this rotated capillary specimen. The powder pattern of tezacaftor Form A from this synchrotron data set has been submitted to ICDD for inclusion in the Powder Diffraction File.

IV. DEPOSITED DATA

The Crystallographic Information Framework (CIF) files containing the results of the Rietveld refinement (including the raw data) and the DFT geometry optimization were deposited with the ICDD. The data can be requested at info@icdd.com.

ACKNOWLEDGEMENTS

Use of the Advanced Photon Source at Argonne National Laboratory was supported by the U.S. Department of Energy, Office of Science, Office of Basic Energy Sciences, under Contract No. DE-AC02-06CH11357. This work was partially supported by the International Centre for Diffraction Data. We thank Lynn Ribaud and Saul Lapidus for their assistance in the data collection, and Andrey Rogachev for the use of computing resources at IIT.

CONFLICTS OF INTEREST

The authors have no conflicts of interest to declare.

Bernstein, J., Davis, R. E., Shimoni, L., and Chang, N. L. (**1995**). "Patterns in hydrogen bonding: functionality and graph set analysis in crystals," Angew. Chem. Int. Ed. Engl. **34**, 1555–1573.

Bravais, A. (**1866**). *Etudes Cristallographiques* (Gauthier Villars, Paris).

Bruno, I. J., Cole, J. C., Kessler, M., Luo, J., Motherwell, W. D. S., Purkis, L. H., Smith, B. R., Taylor, R., Cooper, R. I., Harris, S. E., and Orpen, A. G. (**2004**). "Retrieval of crystallographically-derived molecular geometry information," J. Chem. Inf. Sci. **44**, 2133–2144.

Dassault Systèmes (**2020**). *Materials Studio 2020* (BIOVIA, San Diego, CA).

David, W. I. F., Shankland, K., van de Streek, J., Pidcock, E., Motherwell, W. D. S., and Cole, J. C. (**2006**). "DASH: a program for crystal structure determination from powder diffraction data," J. Appl. Crystallogr. **39**, 910–915.

Donnay, J. D. H. and Harker, D. (**1937**). "A new law of crystal morphology extending the law of Bravais," Am. Mineral. **22**, 446–447.

Dovesi, R., Orlando, R., Erba, A., Zicovich-Wilson, C. M., Civalleri, B., Casassa, S., Maschio, L., Ferrabone, M., De La Pierre, M., D-Arco, P., Noël, Y., Causà, M., and Kirtman, B. (**2014**). "CRYSTAL14: a program for the ab initio investigation of crystalline solids," Int. J. Quantum Chem. **114**, 1287–1317.

Etter, M. C. (**1990**). "Encoding and decoding hydrogen-bond patterns of organic compounds," Acc. Chem. Res. **23**, 120–126.

Friedel, G. (**1907**). "Etudes sur la loi de Bravais," Bull. Soc. Fr. Mineral. **30**, 326–455.

Gates-Rector, S. and Blanton, T. N. (**2019**). "The powder diffraction file: a quality materials characterization database," Powd. Diffr. **34**, 352.

Gatti, C., Saunders, V. R., and Roetti, C. (**1994**). "Crystal-field effects on the topological properties of the electron-density in molecular crystals - the case of urea," J. Chem. Phys. **101**, 10686–10696.

Groom, C. R., Bruno, I. J., Lightfoot, M. P., and Ward, S. C. (**2016**). "The Cambridge structural database," Acta Crystallogr. B: Struct. Sci., Cryst. Eng. Mater. **72**, 171–179.

Hirshfeld, F. L. (**1977**). "Bonded-atom fragments for describing molecular charge densities," Theor. Chem. Acta **44**, 129–138.

Hughes, D. L. (**2019**). "Patent review of synthetic routes and crystalline forms of the CFTR-modulator drugs ivacaftor, lumacaftor, tezacaftor, and elexacaftor," Org. Proc. Res. Dev. **23**, 2302–2322.

Kaduk, J. A., Crowder, C. E., Zhong, K., Fawcett, T. G., and Suchomel, M. R. (**2014**). "Crystal structure of atomoxetine hydrochloride (Strattera), $C_{17}H_{22}NOCl$," Powd. Diffr. **29**, 269–273.

Keshavarz-Shokri, A., Zhang, B., and Alcacio, T. E. (**2016**). "Crystalline form of (R)-1(2,2-difluorobenzo[D][1,3]dioxol-5yl)-N-(1-(2,3-dihyeroxypropyl)-6-fluoro-2-(1-hydroxy-2-methylpropan-2yl)-1H-indol-5yl)cyclopropanecarboxamide," European Patent EP2,563,778B1.

Lee, P. L., Shu, D., Ramanathan, M., Preissner, C., Wang, J., Beno, M. A., Von Dreele, R. B., Ribaud, L., Kurtz, C., Antao, S. M., Jiao, X., and Toby, B. H. (**2008**). "A twelve-analyzer detector system for high-resolution powder diffraction," J. Synch. Rad. **15**, 427–432.

https://doi.org/10.1017/S0885715621000051 Published online by Cambridge University Press

Macrae, C. F., Sovago, I., Cottrell, S. J., Galek, P. T. A., McCabe, P., Pidcock, E., Platings, M., Shields, G. P., Stevens, J. S., Towler, M., and Wood, P. A. (**2020**). "*Mercury 4.0:* from visualization to design and prediction," J. Appl. Crystallogr. **53**, 226–235.

MDI (**2020**). *JADE Pro Version 7.8 (Computer Software)* (Materials Data, Livermore, CA, USA).

O'Boyle, N., Banck, M., James, C. A., Morley, C., Vandermeersch, T., and Hutchison, G. R. (**2011**). "Open Babel: an open chemical toolbox," J. Chem. Informatics **3**, 33.

Peintinger, M. F., Vilela Oliveira, D., and Bredow, T. (**2013**). "Consistent Gaussian basis sets of triple-Zeta valence with polarization quality for solid-state calculations," J. Comput. Chem. **34**, 451–459.

Rammohan, A. and Kaduk, J. A. (**2018**). "Crystal structures of alkali metal (Group 1) citrate salts," Acta Crystallogr. B: Struct. Sci., Cryst. Eng. Mater. **74**, 239–252.

Shields, G. P., Raithby, P. R., Allen, F. H., and Motherwell, W. S. (**2000**). "The assignment and validation of metal oxidation states in the Cambridge Structural Database," Acta Crystallogr. B: Struct. Sci. **56**, 455–465.

Silk Scientific (**2013**). *UN-SCAN-IT 7.0* (Silk Scientific Corporation, Orem, UT).

Sykes, R. A., McCabe, P., Allen, F. H., Battle, G. M., Bruno, I. J., and Wood, P. A. (**2011**). "New software for statistical analysis of Cambridge Structural Database data," J. Appl. Crystallogr. **44**, 882–886.

Toby, B. H. and Von Dreele, R. B. (**2013**). "GSAS II: the genesis of a modern open source all purpose crystallography software package," J. Appl. Crystallogr. **46**, 544–549.

Turner, M. J., McKinnon, J. J., Wolff, S. K., Grimwood, D. J., Spackman, P. R., Jayatilaka, D., and Spackman, M. A. (**2017**). CrystalExplorer17 (University of Western Australia). Available at: http://hirshfeldsurface.net.

van de Streek, J. and Neumann, M. A. (**2014**). "Validation of molecular crystal structures from powder diffraction data with dispersion-corrected density functional theory (DFT-D)," Acta Crystallogr. B: Struct. Sci., Cryst. Eng. Mater. **70**, 1020–1032.

Wang, J., Toby, B. H., Lee, P. L., Ribaud, L., Antao, S. M., Kurtz, C., Ramanathan, M., Von Dreele, R. B., and Beno, M. A. (**2008**). "A dedicated powder diffraction beamline at the advanced photon source: commissioning and early operational results," Rev. Sci. Inst. **79**, 085105.

Wavefunction Inc. (**2020**). Spartan '18 Version 1.4.5, Wavefunction Inc., 18401 Von Karman Ave., Suite 370, Irvine, CA 92612.

https://doi.org/10.1017/S0885715621000051 Published online by Cambridge University Press